Published in final edited form as:
Soft Matter. 2013 December 21; 9(47): . doi:10.1039/C3SM51388B.

Deformation of a Two-domain Lipid Bilayer due to Asymmetric Insertion of Lipid-modified Ras Peptides

Zhenlong Li and **Alemayehu A. Gorfe***
Department of Integrative Biology and Pharmacology, The University of Texas Health Science Center at Houston, 6431 Fannin St., Houston, Texas 77030

Abstract

Ras proteins are attached to the inner leaflet of the plasma membrane via a lipid-modified anchor. Membrane-bound Ras proteins laterally segregate into nanoscale signaling platforms called nanoclusters. It has been shown that the membrane domain preference of Ras nanoclusters varies with the nature of lipidation but their effect on the membrane has not been well understood. To investigate the effect of Ras insertion on membrane structure, we carried out numerous coarse-grained molecular dynamics (CGMD) simulations on a two-domain DPPC/DLiPC/cholesterol lipid bilayer in which different number and type of H-ras peptides were attached on one side. We have shown previously that this lipid mixture forms co-existing liquid-ordered/liquid-disordered (L_o/L_d) domains and that different H-ras peptides form clusters that variously accumulate at the L_o/L_d regions or the boundary between them. Here we show that asymmetric insertion of each of these peptides induces a vertical relative displacement of the domains and deforms the bilayer, with the domain boundary serving as the center of deformation. The extent of the deformation, however, varies with the type and number of lipid modification. This is because the number and type of the Ras lipid tails determines the degree to which the stress caused by asymmetric peptide insertion is relieved by inter-leaflet cholesterol transfer and lipid tilt. In addition, we have characterized the mechanism of bilayer deformation based on the collective effect of the Ras peptides on inter-leaflet surface area, pressure profile and line tension differences. This allowed us to elucidate how Ras lipid modification affects membrane geometry and how a two-domain bilayer adjusts its shape through boundary deformation. The result contributes to a better understanding of Ras signaling platforms and highlights some of the mechanisms by which a multi-domain membrane responds to external perturbation.

Keywords

Ras; lipid modification; membrane domain; molecular dynamics; membrane shape

1. Introduction

Ras proteins act as molecular switches in cell signaling pathways to regulate cell growth, proliferation and differentiation[1]. They are normally anchored to the inner surface of the plasma membrane by a lipid-modified C-terminus, which also plays an important role in the formation of nanoscale signaling platforms called nanoclusters[2]. The three human Ras

Corresponding Author: Alemayehu A Gorfe, Tel: 713-500-7538, Alemayehu.G.Abebe@uth.tmc.edu.

Supplementary Information
Supplementary Information about the bilayer density profile, shape for bilayers containing different numbers of tH and its variants and inter-leaflet cholesterol transfer are available.

isoforms (H-, N-, K-Ras) share a highly conserved catalytic domain but differ in sequence as well as in the number and type of lipid modification at the C-terminus[1]. This variation in lipid modification has been suggested as the primary reason for the non-overlapping distribution of nanoclusters of different Ras isoforms in the plasma membrane[2, 3]. A similar behavior has been observed in model membranes with co-existing raft-like liquid-ordered (L_o) and non-raft liquid-disordered (L_d) lipid domains[4, 5]. K-Ras, which contains a single farnesyl modification, prefers the L_d domain enriched with unsaturated lipids[5]. N-ras is modified by a palmitoyl and a farnesyl lipid and prefers the L_o/L_d domain boundary[4]. The dually palmitoylated and farnesylated H-ras reportedly localizes at the L_o domain[6].

Membrane binding[7–13] and nanoclustering[2, 3, 6, 14, 15] of Ras proteins have been relatively well characterized. Fewer studies have focused on how Ras insertion affects the structure of the host membrane[16–20]. For instance, using solid state NMR and molecular dynamics simulations, Vogel *et al* investigated N-Ras and a peptide representing its lipidated C-terminus in different bilayer systems[16, 21, 22]. They showed that the local lipid packing is slightly affected by N-ras insertion. Similarly, our previous studies on the isolated H-Ras lipid anchor and full-length H-ras in a DMPC bilayer have suggested small structural perturbation of the bilayer[18, 19]. In another study of the K-ras lipid anchor in a mixed bilayer, we found that the positively charged peptide clusters negatively charged POPG lipids and induces local thinning in the bilayer[20]. These observations had shed some light on the effect of monomeric Ras on simple model membranes. The impact of clustered Ras proteins on more complex heterogeneous membranes remains unknown.

In previous reports, we used CGMD to investigated the nanoclustering behavior of the minimal membrane binding motif of H-ras (tH), and its mutants with different lipid modification (Fig. 1), embedded in one leaflet of a DPPC/DLiPC/cholesterol bilayer that forms L_o/L_d domains[14, 15, 23]. Accumulation of tH nanoclusters in a specific region of an initially symmetric bilayer led to deformation. This observation was difficult to explain based solely on the steric effect of asymmetric insertion[14]. As a result, the physical basis for the deformation was not fully explored. The primary goal of this work was to further probe this issue using a detailed analysis of our CGMD trajectories.

The response of a multi-domain membrane to Ras insertion can be complicated by the presence of the domain boundary. This is because the free energy of a multi-domain membrane has contributions from both domain bending and boundary line energies[24] and therefore the equilibrium shape can be tuned by changes in individual bending moduli or line tension. For instance, increasing the line tension can lead to contraction or even budding of the central domain from the surrounding domain, which reduces the inter-domain contact length[24–26]. Although a molecular-level picture of a multi-domain membrane is beyond the resolution limit of most current experimental techniques, continuum elasticity theory and CGMD simulations have been extensively used to study the link between structure and mechanics in multi-domain membranes[27, 28]. According to these studies, a compositionally symmetric planar bilayer containing L_o and L_d domains is mirror-symmetric across the bilayer mid-plane and there is a smooth thickness change at the transition region between the domains[27, 28]. How such a membrane would respond to an asymmetric insertion of laterally segregated membrane proteins remains an open question. Herein we extended our previous work to systematically investigate the deformation of a bilayer upon an asymmetric insertion of Ras peptides that harbor different number and type of lipid modifications. The results provided a mechanistic picture of how clustered lipidated peptides remodel the host membrane.

2. Methods

Model and CGMD simulations

Mixed lipid bilayers with and without Ras peptides were modeled by the MARTINI force field version 2.0[29, 30] (Fig. 2) and simulated by the GROMACS package version 4.0[31]. Details of the models and simulation protocol can be found in our previous reports[14, 15]. Briefly, four sets of simulations were conducted (Supplementary information Table S1). The first is a compositionally symmetric reference bilayer made up of 960 DPPC, 576 DLiPC and 384 cholesterol molecules[14]. In the second set 16, 32, 48 and 64 tH peptides were embedded into the lower leaflet of a bilayer with identical lipid composition as in the reference bilayer[15]. In the third set the cholesterol fraction was varied between 0%, 11%, 20% and 27% keeping a fixed concentration of 64 tH peptides[15]. The final set of simulations involved four mutant tH peptides that have one or two lipid modifications[14] (Fig. 1). Each simulation was run for 40μs effective time.

Data analysis

A combination of in-house scripts and GROMACS[31] tools were used to analyze the well-equilibrated 24–403s portion of each trajectory. Equilibrium structural properties of the bilayer were calculated by binning the system into equal slabs in the direction perpendicular to the domain boundary line with the center of the L_d domain as origin (after removal of domain center motion). Bilayer shapes were characterized based on the average *z*-position of the phosphate beads and the terminal beads of the lipid tails. The bilayer structure was characterized using the conformation of individual lipid molecules. As commonly done in the theory of membrane elasticity[32–34], we decomposed the bilayer elastic deformation into contributions from area expansion/compression, lipid tilt and lipid splay. The latter two deformation modes were analyzed in detail because they are more applicable to a tensionless bilayer[27]. Lipid splay was monitored by the average width (w) and height (h) of individual lipids, calculated as the distance between the terminal beads of the tails and between the phosphate group and the center-of-mass of the two tail terminal beads, respectively. Local lipid tilt was monitored by the average tilt angle (φ) of individual lipids, defined as the deviation of the lipid tail director vector **n** (the head-to-tail principal axis excluding the choline bead) from the normal of the local monolayer surface **N**. Note that φ is different from the lipid orientation angle ϕ in our previous report[14], which was the deviation of the lipid head-to-tail principal axis from the global normal of the bilayer surface.

3. Results

The shape and structure of the bilayer without any peptide is described first, followed by bilayers that contain peptides harboring different type and number of lipid modification. We then turn to the mechanism of bilayer deformation due to asymmetric peptide insertion.

3.1 Structure of the reference planar bilayer with coexisting L_o/L_d domains

The equilibrated tH-free bilayer has two striped domains: a DPPC/cholesterol-enriched L_o domain and a DLiPC-enriched L_d domain. Each monolayer of the L_o domain was thicker than the corresponding L_d monolayer by ~0.5nm, as has been shown previously[14]. The bilayer was mirror symmetric across the common mid-plane of the two domains (Fig. 3a) and exhibited a strong inter-leaflet domain registration[28], as seen from the nearly identical lipid density profiles at the two leaflets (Fig. S1a). The tightly packed lipids in the L_o domain were taller (large h) and their tails less spread (small w) than those in the L_d domain (Fig. 3b). The bilayer shape, density, h, and w all showed a smooth transition at the boundary regions. Lipids at the narrow (~4.7nm) L_o/L_d domain boundary region have to slightly tilt away from the local monolayer surface normal to accommodate the curved

surface (Fig. 3c). Lipids in the boundary region experienced larger fluctuation (see the standard deviations in the plots of Fig. 3a) due to the relative motion of the domains along the bilayer normal.

3.2 Peptide-induced bilayer deformation

Insertion of 64 tH peptides into the lower leaflet induced curvature at both leaflets (Fig. 4). Both domains were nearly flat at their centers but underwent vertical displacement relative to each other. For instance, the mid-plane of the L_o domain was displaced by ~1.5nm at the center relative to the tH-free bilayer (Fig. 4a, see also Fig. 5a for a schematic explanation). This vertical displacement increased the vertical distance between the L_d and L_o surfaces from ~0.5nm (tH-free) to ~1.9nm (tH-bound) in the lower leaflet. The corresponding increase in the upper leaflet was smaller (from 0.5 to 1.0nm). The displacement mainly occurred at the domain boundary (Fig. 4a). The domain boundary, where the shape fluctuation was highest, is therefore the center for deformation. This was confirmed by the finding that a bilayer containing the same numbers of DPPC, DLiPC and tH but lacking cholesterol (hence no stripped domains) remained essentially flat (Fig. S2).

There were fewer cholesterol molecules in the lower leaflet than in the upper due to displacement by tH (Fig. S1b). Moreover, despite the overall similarities in the density distributions of DPPC and DLiPC in the two monolayers, there were some important differences. First, the distributions did not overlap as well as they did in the tH-free bilayer (Fig. S1a), suggesting reduced inter-leaflet domain registration. Secondly, the slightly smaller DLiPC density in the upper L_d domain suggested comparatively tighter packing in the corresponding region of the lower monolayer. This was reversed in the case of the DPPC lipids at the L_o domain. These observations suggest that tH binding had a differential effect, albeit small, on the packing behavior of lipids at the two monolayers of each domain. This resulted in larger w and smaller h for the upper monolayer, especially in the narrow L_d and the boundary regions (Fig. 4b). More dramatic change was found for φ (Fig. 4c), where lipids with large φ populate the entire domain boundary of the lower leaflet, suggesting that the domain boundary is the major deformation center. Taken together, these results show that the lower leaflet undergoes a large deformation compared to the upper leaflet, and that the bilayer deformed mainly through lipid tilt instead of splay. This is consistent with a previous prediction that the tilt mode, which is only weakly coupled across monolayers, can effectively modulate bilayer shape[35].

The lateral dimension and hence domain width of the bilayer was only slightly different among simulations with different tH concentration (table S1). Therefore, we used domain displacement to test the dependence of bilayer deformation on peptide concentration, (Fig. 5a, and S3). The corresponding average vertical displacement (Δh) is shown in Fig. 5b for bilayers containing different amount of tH peptides. One can see that the extent of bilayer deformation varies with peptide concentration so that the displacement progressively increases with the number of tH. For instance, at the lowest tH concentration (16 peptides) the upper surface was nearly flat with no height difference between the L_d and L_o domain, while for N_p=64 Δh_m reached ~1.5nm. Moreover, the domain displacements (Fig. 6c and S4), varied with the type of lipid modification and hence the domain preference of the peptides. In fact, the extent of bilayer deformation significantly depend on the domain-preference of the peptides[14], with the L_o-localized *de*-Fa186 causing the largest displacement and the L_d-localized *de*-Pa181/184 causing the least displacement. Peptides containing farnesyl and at least one palmitoyl, and hence segregating to the domain boundary, have similar and intermediate effect on the bilayer shape. Taken together these results indicate that bilayer deformation is a function of both the concentration and domain preference of the lipidated Ras peptides. Moreover, there appear to be an intriguing trend

that suggests a progressively larger effect on the bilayer structure as the peptides' domain preference shifts from the disordered L_d to the ordered L_o domain.

3.3 Mechanism of bilayer deformation

Inter-leaflet compositional asymmetry—No flip-flop of DPPC or DLiPC was observed within the time scale of the simulations. Cholesterol has a faster flip-flop rate[28, 36] and can undergo inter-leaflet transfer upon peptide insertion. This was the case in all tH-containing bilayers where a fraction of the lower leaflet cholesterol has moved to the upper leaflet at the early stage of the simulation (Fig. S5). The number of transferred cholesterols was found to be proportional to the total number of peptide lipid tails (slope = 1/3, see Fig. 6a). Thus, on average 3 tH tails expelled one cholesterol and thereby minimized the volume difference between the two leaflets. As cholesterol increases monolayer bending rigidity[37], such an inter-leaflet cholesterol transfer should lead to a larger bending rigidity of the upper leaflet. On the other hand, experiments[38] and MD simulation[36] have shown that rapid inter-leaflet re-equilibration of cholesterol reduces the overall membrane stress and allows membrane shape relaxation. Taken together these results suggest that without the relaxation by cholesterol transfer a larger bilayer curvature would have occurred.

To test if cholesterol flip-flop compensated for the entire inter-leaflet volume difference, we looked at changes in the box volume (ΔV) upon increasing the number of cholesterol or tH in the system. We found a 4-fold larger ΔV per peptide than ΔV per cholesterol (Fig. 6a). Thus, cholesterol transfer only partly reduced the inter-leaflet volume difference. This suggests that the remaining excess volume in the lower leaflet, largely due to the adsorption of the peptide backbone and the non-lipidated side chains in the lipid-water interface of the lower leaflet, should be responsible for the observed bilayer deformation (discussed in the previous section).

Monolayer area difference due to peptide insertion—Fig. 6b shows that the backbone resides near the head-group region and therefore can contribute to monolayer surface area expansion. We computed monolayer surface area (A_s) from the product of the average length of the monolayer surface curves (Fig. 3a, 4a and S4) (i.e., the side perpendicular to the boundary line) and the length of the box parallel to the boundary line. Fig. 7a shows that, for each monolayer, A_s increases linearly with the peptide concentration. The surface area expansion was ~23% larger for the lower monolayer (~0.64nm^2/tH) than the upper (~0.49nm^2/tH). These values are much greater than ΔA/cholesterol (~0.03–0.1nm^2, derived from Fig. 7a (inset)). Considering the 1:1 expulsion ratio of cholesterol to tH, it is clear that the upper leaflet area expansion was much higher than the possible contribution from the transferred cholesterol molecules.

It is not feasible to precisely resolve the partial specific area of each constituent in such a complex mixture[39]. However, it is possible to determine the average effect of tH and its partially de-lipidated variants on the monolayer areas. Fig. 7b shows that the surface area varies both with the number and type of lipid modification. The triply lipidated tH caused the largest increase in A_s while the variant with just farnesyl (*de*-Pa181/184) had the smallest effect. The doubly lipidated *de*-Pa181, *de*-Pa184 and *de*-Fa186 had an intermediate effect, with *de*-Fa186 causing the minimal area increase among them. The reason for the later is that the insertion depth of *de*-Fa186 into the tightly packed L_o domain was less than those of *de*-Pa181 or *de*-Pa184 (Fig. 6b). This suggests that insertion depth of the tails and backbone of the peptides affects the bilayer surface area. Moreover, tH and its variants have positive spontaneous curvature due to the volume difference between their hydrophobic tail and polar head. Coupled with the expulsion of cholesterol molecules, which have intrinsic negative curvature, the positive curvature of the peptides can enhance the spontaneous

curvature of the lower leaflet. To further investigate this issue, below we discuss the consequence of the excess volume/surface area in the lower leaflet, plus the difference in the shape and distribution of the peptides and cholesterol, on the properties of the bilayer.

Pressure profile, surface tension and line tension—A potential consequence of inter-leaflet compositional asymmetry is to induce pressure profile asymmetry[36, 40]. The pressure profile of the tH-free bilayer, calculated along the z-direction[41], was symmetric across the mid-plane (Fig. 8a). In the presence of tH, the magnitude of the negative peak in the lower leaflet was reduced and shifted toward the surface in a concentration dependent manner. Correspondingly, the pressure profile in the upper leaflet increased and the negative peak shifted toward the core. The effect is less pronounced for the two lowest tH concentrations (Fig. 8a). The type of lipid modification (and hence domain preference) also had a significant effect on the pressure profile (Fig. 8b). The single-tailed *de*-Pa181/184 had the minimal effect since it preferred the loosely packed L_d domain.

We have also calculated monolayer surface tension (γ) from the pressure profiles (Fig. 8a&b, insets). As expected, γ was close to zero for the symmetric tH-free and the nearly symmetric ternary bilayer with 16 tHs (Fig. 8a) but it changed dramatically when the number of tH was 32 or higher. Consistent with the opposite bending of the two monolayers γ was positive for the upper leaflet and negative for the lower leaflet. This suggests that the lower leaflet drives the deformation while the coupled upper leaflet responds by expanding its area, which is consistent with our conclusion from monolayer surface area analysis. Overall, tH caused the largest change in surface area and inter-leaflet surface tension while *de*-Pa181/184 had the smallest effect on both (Figs. 8b and 8b inset). Note that because the bilayer was tensionless the sum of monolayer surface tensions is close to zero in every case.

A smooth L_d/L_o transition at domain boundaries can reduce exposure of the tails of the L_o lipids[27]. This was the case in the tH-free bilayer (Fig. 3a), where a progressive adjustment of lipid conformation and composition within the ~5nm-wide boundary region ensured a smooth transition. The line tension (σ) at the boundary was 4.5±0.5pN[14] per monolayer, as estimated from boundary fluctuation analysis[14, 42]. In most cases tH binding had negligible effect on σ of the upper monolayer but generally reduced σ of the lower monolayer (Fig. 9a). tH variants affected σ of either monolayer, depending on the type of lipid modification and/or their domain preference (Fig. 9b). For instance, the L_d-enriched *de*-Pa181/184 reduced the line tension of the upper leaflet whereas the L_o-enriched *de*-Fa186 affected the lower leaflet. The common feature among all of the peptides is that they caused an imbalance in the monolayer line tensions.

4. Discussion

In this work we have investigated how asymmetric insertion and domain-specific aggregation of lipid-modified Ras peptides affect the geometry of a two-domain bilayer. Design of the model system was based on the fact that Ras proteins are attached to the inner surface of the plasma membrane. Once inserted, the peptides laterally segregate into different membrane domains[2, 9]. Starting from an initially symmetric bilayer and monitoring its evolution over time, we were able to characterize the effect of different Ras peptides to the bilayer topology. Analysis of the bilayer volume and surface area provided details about the distinct effects of the peptide backbone and lipid tails. Though lipid modification dictates domain preference, the insertion depth of the backbone also plays an important role not only in peptide-membrane interaction but also in affecting membrane geometry. It is important to mention that previous studies indicated the catalytic domain of full-length Ras proteins may also interact with the membrane surface and hence affect bilayer structure[43, 44], which is the subject of future studies.

In recent years, N- and K-ras proteins have been successfully incorporated into heterogeneous model lipid membranes with coexisting L_o and L_d domains[5,9]. Our observation that palmitolyation drives Ras towards L_o domain and farnesylation drives Ras towards L_d domain agrees well with the experimental observations that N-ras prefers the domains boundary and K-ras prefers the L_d domain[5,9]. With the insertion of Ras onto the surface of a giant unilamellar vesicle with L_o/L_d co-existence, it is possible to test our predictions by comparing the vesicle shape with a Ras-free vesicle. For example, when localizing at the domain boundary, H- and N-ras may increase the positive spontaneous curvature of the host monolayer and decrease the domain boundary line tension and eventually alter the vesicle shape. It is expected that such effect would heavily depend on the concentration of Ras proteins.

Our investigation of the various modes of bilayer deformation upon insertion of different Ras peptides provided important information about the structural characteristics of a two-domain bilayer. For a symmetric lipid bilayer with co-existing L_o/L_d domains, mirror symmetry across the mid-plane was maintained and the line tension was the same for the two monolayers. Upon an asymmetric insertion of Ras peptides, however, the bilayer adjusted its shape via a fast inter-leaflet cholesterol re-distribution and enhanced lipid tilt. The bilayer tends to deform through the domain boundary irrespective of a peptide's domain preference. This result highlights the important role of the boundary in facilitating membrane shape adjustment. The L_o domain is more rigid and therefore tends to move or deform as a patch relative to the L_d domain, subjecting the stress reservoir boundary region to deformation. Absorption of stress is consistent with the observed high probability of budding and vesiculation through domain boundaries in model membranes[24–26].

5. Conclusion

In summary, the influence of the membrane-binding motif of Ras proteins on bilayer structure described in this study provides a mechanistic insight into how lipid-modified proteins affect membrane geometry. By analyzing the deformation of a two-domain bilayer upon an asymmetric peptide insertion we were able to show that the domain boundary plays an essential role for membrane geometry modulation. These insights help link predictions from continuum elastic membrane models[24, 25, 27] and observations from experiments[26] on how multi-domain membranes respond to perturbation.

Supplementary Material

Refer to Web version on PubMed Central for supplementary material.

Acknowledgments

We thank the National Institutes of Health Institute of General Medicine (RO10GM100078) and the UThealth Innovation for cancer Prevention Research Postdoctoral Fellowship by the UThealth School of Public Health and Cancer Prevention and Research Institute of Texas (RP101503) for financial support, and the Texas Advanced Computing Center for computational resources. We also thank members of the Gorfe laboratory for fruitful discussions.

References

1. Karnoub AE, Weinberg RA. Nat Rev Mol Cell Biol. 2008; 9:517–531. [PubMed: 18568040]
2. Abankwa D, Gorfe AA, Hancock JF. Semin Cell Dev Biol. 2007; 18:599–607. [PubMed: 17897845]
3. Hancock JF. Nat Rev Mol Cell Biol. 2003; 4:373–384. [PubMed: 12728271]

4. Nicolini C, Baranski J, Schlummer S, Palomo J, Lumbierres-Burgues M, Kahms M, Kuhlmann J, Sanchez S, Gratton E, Waldmann H, Winter R. J Am Chem Soc. 2006; 128:192–201. [PubMed: 16390147]
5. Weise K, Kapoor S, Denter C, Nikolaus J, Opitz N, Koch S, Triola G, Herrmann A, Waldmann H, Winter R. J Am Chem Soc. 2011; 133:880–887. [PubMed: 21141956]
6. Plowman SJ, Muncke C, Parton RG, Hancock JF. Proc Natl Acad Sci U S A. 2005; 102:15500–15505. [PubMed: 16223883]
7. Brunsveld L, Waldmann H, Huster D. BBA-Biomembranes. 2009; 1788:273–288. [PubMed: 18771652]
8. Gorfe AA. Curr Med Chem. 2010; 17:1–9. [PubMed: 19941482]
9. Weise K, Huster D, Kapoor S, Triola G, Waldmann H, Winter R. Faraday Discuss. 2013; 161:549–561. [PubMed: 23805758]
10. Gorfe AA, Pellarin R, Caflisch A. J Am Chem Soc. 2004; 126:15277–15286. [PubMed: 15548025]
11. Gorfe AA, Babakhani A, McCammon JA. Angew Chem Int Ed Engl. 2007; 46:8234–8237. [PubMed: 17886310]
12. Gorfe AA, McCammon JA. J Am Chem Soc. 2008; 130:12624–12625. [PubMed: 18761454]
13. Gorfe AA, Baron R, McCammon JA. Biophys J. 2008; 95:3269–3277. [PubMed: 18621822]
14. Janosi L, Li Z, Hancock JF, Gorfe AA. Proc Natl Acad Sci U S A. 2012; 109:8097–8102. [PubMed: 22562795]
15. Li Z, Janosi L, Gorfe AA. J Amer Chem Soc. 2012; 134:17278–17285. [PubMed: 22994893]
16. Vogel A, Reuther G, Weise K, Triola G, Nikolaus J, Tan KT, Nowak C, Herrmann A, Waldmann H, Winter R, Huster D. Angew Chem Int Ed Engl. 2009; 48:8784–8787. [PubMed: 19830755]
17. Vogel A, Reuther G, Roark MB, Tan KT, Waldmann H, Feller SE, Huster D. BBA-Biomembranes. 2010; 1798:275–285. [PubMed: 19819220]
18. Gorfe AA, Babakhani A, McCammon JA. J Am Chem Soc. 2007; 129:12280–12286. [PubMed: 17880077]
19. Gorfe AA, Hanzal-Bayer M, Abankwa D, Hancock JF, McCammon JA. J Med Chem. 2007; 50:674–684. [PubMed: 17263520]
20. Janosi L, Gorfe AA. Biophys J. 2010; 99:3666. [PubMed: 21112291]
21. Vogel A, Katzka CP, Waldmann H, Arnold K, Brown MF, Huster D. J Am Chem Soc. 2005; 127:12263–12272. [PubMed: 16131204]
22. Vogel A, Tan KT, Waldmann H, Feller SE, Brown MF, Huster D. Biophys J. 2007; 93:2697–2712. [PubMed: 17557790]
23. Li Z, Gorfe AA. Small GTPase. 2012; 3:244–247.
24. Lipowsky R. J Phys II. 1992; 2:1825–1840.
25. Jülicher F, Lipowsky R. Phys Rev Lett. 1993; 70:2964–2967. [PubMed: 10053698]
26. Baumgart T, Hess ST, Webb WW. Nature. 2003; 425:821–824. [PubMed: 14574408]
27. Kuzmin PI, Akimov SA, Chizmadzhev YA, Zimmerberg J, Cohen FS. Biophys J. 2005; 88:1120–1133. [PubMed: 15542550]
28. Risselada HJ, Marrink SJ. Proc Natl Acad Sci U S A. 2008; 105:17367–17372. [PubMed: 18987307]
29. Marrink SJ, Risselada HJ, Yefimov S, Tieleman DP, de Vries AH. J Phys Chem B. 2007; 111:7812–7824. [PubMed: 17569554]
30. Monticelli L, Kandasamy SK, Periole X, Larson RG, Tieleman DP, Marrink SJ. J Chem Theory Comput. 2008; 4:819–834.
31. Hess B, Kutzner C, Van Der Spoel D, Lindahl E. J Chem Theory Comput. 2008; 4:435–447.
32. Helfrich W. Z naturforsch. 1973; 28:693–703.
33. Hamm M, Kozlov M. Eur Phys J B. 1998; 6:519–528.
34. Hamm M, Kozlov M. Eur Phys J E. 2000; 3:323–335.
35. Seifert U, Shillcock J, Nelson P. Phys Rev Lett. 1996; 77:5237–5240. [PubMed: 10062750]
36. Yoo J, Cui Q. Biophys J. 2009; 97:2267–2276. [PubMed: 19843459]

37. Hofsäß C, Lindahl E, Edholm O. Biophys J. 2003; 84:2192–2206. [PubMed: 12668428]
38. Bruckner R, Mansy S, Ricardo A, Mahadevan L, Szostak J. Biophys J. 2009; 97:3113–3122. [PubMed: 20006948]
39. Edholm O, Nagle JF. Biophys J. 2005; 89:1827–1832. [PubMed: 15994905]
40. Esteban-Martín S, Risselada HJ, Salgado J, Marrink SJ. J Amer Chem Soc. 2009; 131:15194–15202. [PubMed: 19795891]
41. Ollila OHS, Risselada HJ, Louhivuori M, Lindahl E, Vattulainen I, Marrink SJ. Phys Rev Lett. 2009; 102:78101.
42. Esposito C, Tian A, Melamed S, Johnson C, Tee SY, Baumgart T. Biophys J. 2007; 93:3169–3181. [PubMed: 17644560]
43. Abankwa D, Hanzal-Bayer M, Ariotti N, Plowman SJ, Gorfe AA, Parton RG, McCammon JA, Hancock JF. EMBO J. 2008; 27:727–735. [PubMed: 18273062]
44. Abankwa D, Gorfe AA, Inder K, Hancock JF. Proc Natl Acad Sci U S A. 2010; 107:1130–1135. [PubMed: 20080631]

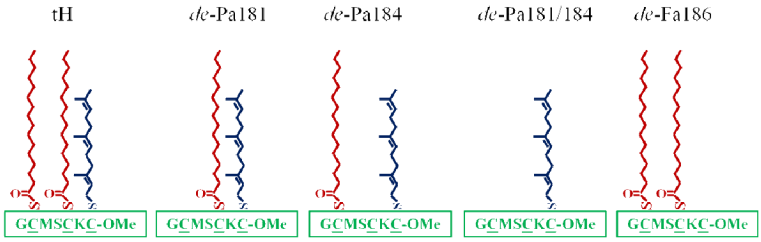

Fig. 1.
Sequence and lipid modification of the H-ras peptides used in this study.

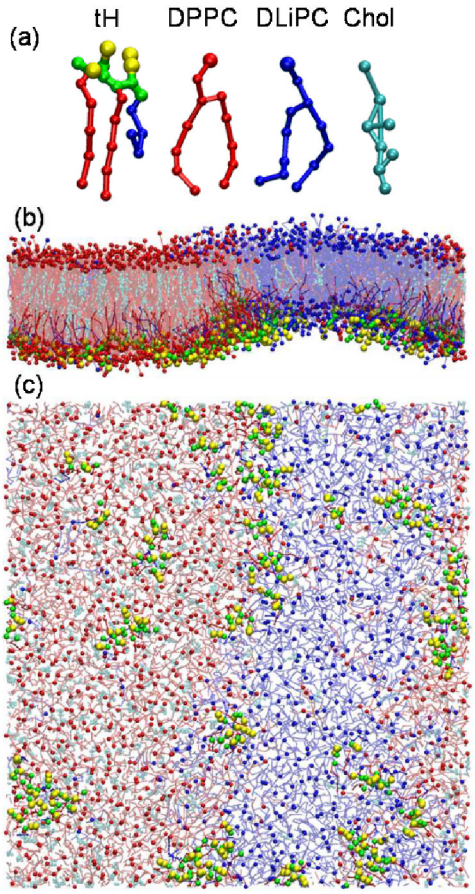

Fig. 2.

Molecular models and snapshots. (a) Coarse-grained molecular model of the tH peptide and lipids. (b) Side view of the bilayer from the domain boundary direction. (c) Bottom view of the bilayer. Water molecules are not shown. Snapshots were taken at t=24μs for the system with 64 tH peptides embedded in a 5:3:2 DPPC:DLiPC:Chol bilayer.

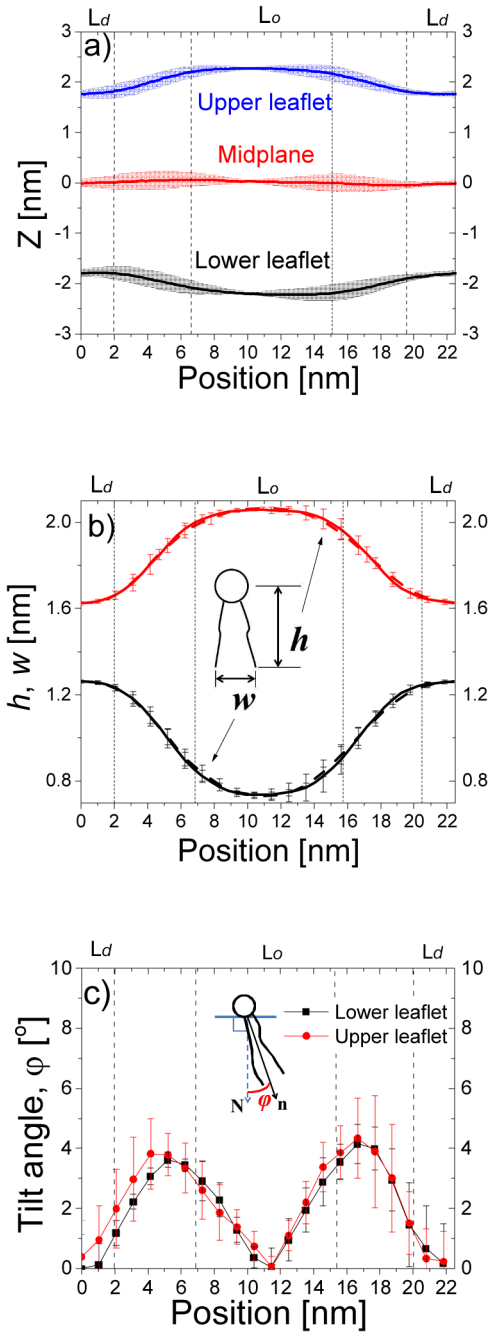

Fig. 3.

Shape and structure of the tH-free bilayer along the direction perpendicular to the domain boundary. (a) Bilayer shape described by the monolayer surfaces and the mid-plane. Each monolayer surface was represented by the average z-position of its phosphate beads, and the mid-plane by the average z-position of the last lipid tail beads of both monolayers. (b) Lipid height (*h*) and width (*w*) for the upper (dash line) and lower (solid line) monolayer. (c) Lipid tilt angle of the upper (square) and lower (circle) monolayer. Errors were calculated by block-averaging after separating the 16-μs trajectory evenly into 5 time blocks.

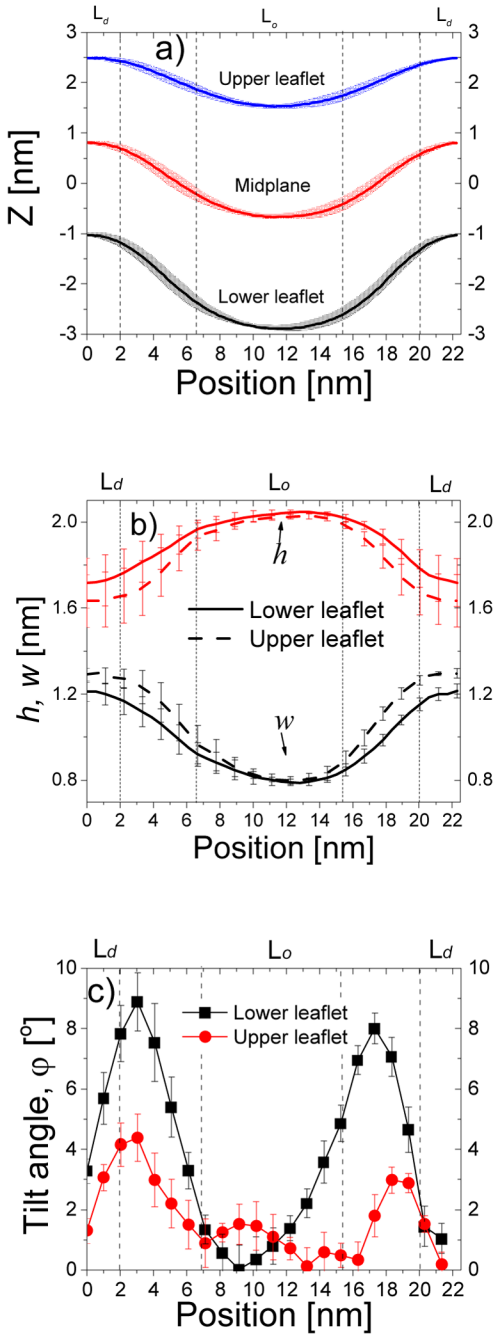

Fig. 4.

Shape and structure of a bilayer containing 64 tH peptides along the direction perpendicular to the domain boundary. (a) Shape of the bilayer described by monolayer surfaces and the mid-plane. Each monolayer surface was represented by the average *z*-position of its phosphate beads, and the mid-plane by the average z-position of the last lipid tail beads of both monolayers. (b) Lipid height (*h*) and width (*w*) for the upper (dash line) and lower (solid line) monolayer. (c) Lipid tilt angle of the upper (square) and lower (circle) monolayer. Errors were calculated as described in Fig. 3.

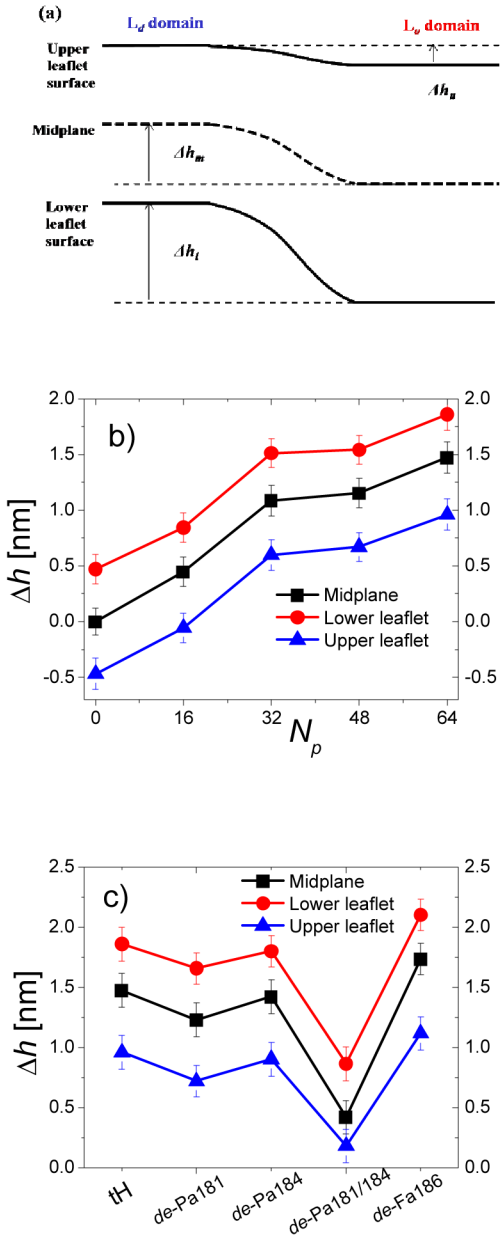

Fig. 5.

Peptide-induced bilayer deformation. (a) Schematic representation of the vertical distance between the two domains of the lower leaflet (h_l), midplane (h_m) and upper leaflet (h_u). (b) Vertical domain displacements for bilayers containing different number of tH peptides. (c) Vertical domain displacements for bilayers containing the same number of tH peptides with different types of lipid modifications. Errors were calculated as described in Fig. 3.

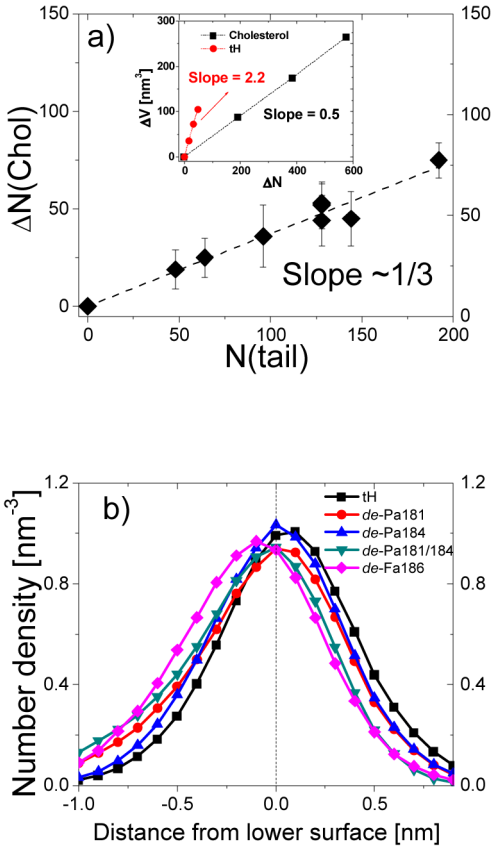

Fig. 6.

Monolayer composition asymmetry. (a) Differences in the average cholesterol number between the upper and the lower leaflet versus the number of peptide lipid tails. Errors for ΔN(Chol) were calculated by averaging over the 16-μs trajectory. Inset: simulation box volume increase versus the number of cholesterol and tH molecules. The volume difference due to cholesterol was calculated for systems containing increasing amount of cholesterol and 960 DPPC, 576 DLiPC and 64 tH molecules. The volume difference due to tH molecule was calculated for the bilayers containing increasing amount of tH and 960 DPPC, 576 DLiPC and 384 cholesterol molecules. Errors for the volume are within the range of the symbols. (b) Number density profiles of the peptide backbone beads along the z-dimension, with the local monolayer surface defined as the origin.

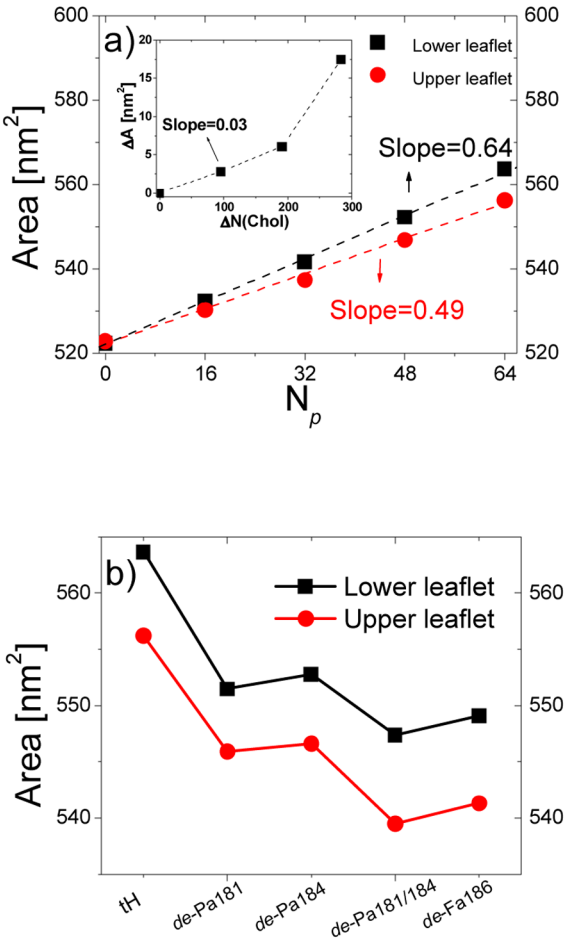

Fig. 7.

Monolayer surface area. (a) Monolayer surface area increase due to insertion of different numbers of tH molecules at the lower leaflet. Inset: the corresponding monolayer surface area. (b) Monolayer surface area increase due to insertion of the same number of peptides that have different lipid modifications. Errors were calculated as described in Fig. 3 and within the range of the symbols.

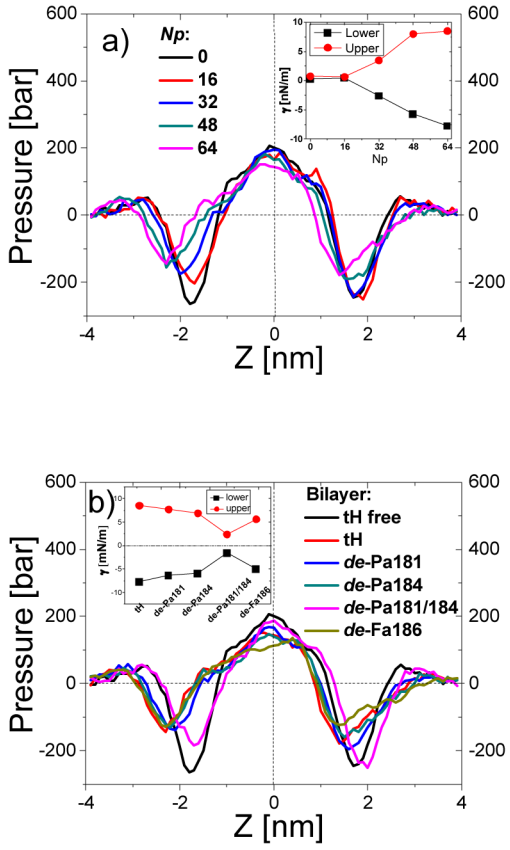

Fig. 8.

Bilayer pressure profile and monolayer surface tension. (a) Bilayer pressure profile along the z-direction and monolayer surface tension (inset) for bilayers containing different amounts of tH peptides. (b) Bilayer pressure profile along the z-driection and monolayer surface tension (inset) for bilayers containing 64 peptides with different lipid modifications.

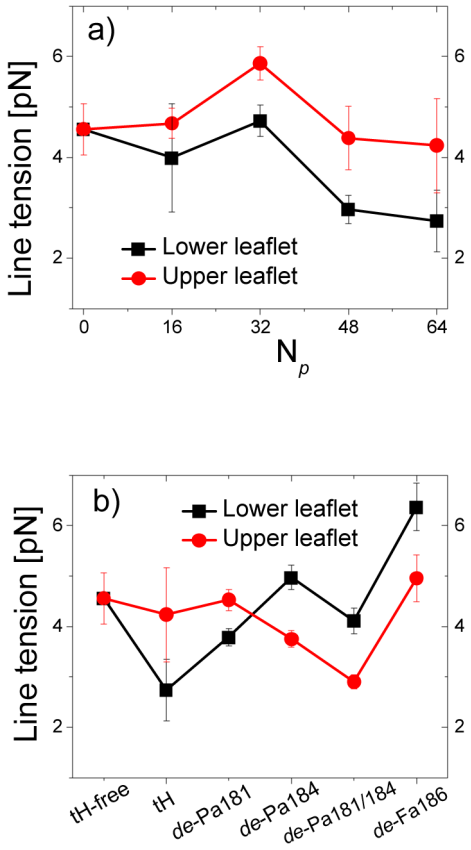

Fig. 9.

Line tension. (a) Monolayer line tension for bilayers containing different amounts of tH peptides. (b) Monolayer line tension for bilayers containing the same amount (N_p=64) of peptides with different lipid modifications. Errors were calculated as described in Fig. 3.